THE JOURNAL OF PHYSICAL CHEMISTRY C

ARTICLE

pubs.acs.org/JPCC

Aromatic and Aliphatic Thiol Self-Assembled Monolayers on Au: Anchoring and Delivering Copper Species

R. Urcuyo,[†] E. Cortés,[‡] A. A. Rubert,[‡] G. Benitez,[‡] M. L. Montero,[†] N. G. Tognalli,[§] A. Fainstein,[§] M. E. Vela,[*,‡] and R. C. Salvarezza[‡]

[†]Electrochemistry and Chemistry Energy Center (CELEQ), Chemistry School, University of Costa Rica, San José, Costa Rica

[‡]The Research Institute of Theoretical and Applied Physical Chemistry (INIFTA), La Plata National University-CONICET (National Scientific and Technical Research Council), Sucursal 4 Casilla de Correo 16, 1900 La Plata, Argentina

[§]Bariloche Atomic Center and Balseiro Institute, Atomic Energy National Commission, 8400 S. C. de Bariloche, Río Negro, Argentina

Supporting Information

ABSTRACT: The immobilization of dinuclear copper(II) acetate complexes ($Cu_2(CH_3COO)_4 \cdot 2H_2O$) on self-assembled monolayers (SAMs) of different aliphatic and aromatic thiols with oxygen and nitrogen donors at the end group is investigated on preferentially oriented (111) gold surfaces (Au(111)). The Cu species are immobilized at the outer plane of these terminal groups by the interaction of the terminal moiety of the functionalized SAMs. The highest electrochemical activity for the Cu(II)/Cu(I) redox couple is found for the metallic complexes immobilized on SAMs of short thiols, irrespective of their aliphatic or aromatic character, or the nature of the terminal group of the linking molecule, suggesting that direct tunneling is the main path for charge transfer to the Au substrate. Even though a progressive demetalation of the copper acetate complex immobilized on N-terminated SAMs by the release of Cu ions to the solution is induced by repeated potential scans, this process is negligible for Cu species immobilized on O-terminated thiols. The Cu(I)/Cu(0) reaction is not observable in the overall potential range where thiol SAMs are stable on the Au(111) surface. In contrast, this reaction is clearly visible by using nanostructured Au, a substrate that exhibits a wider potential window of SAM stability and larger capture areas than ordered smooth metal surfaces. Finally, spatial 2D and 3D confinement of the copper complex can be performed by SAMs of mixed thiols with different immobilization abilities and by building complex electrochemically active supramolecular structures. Our results are important to understand the behavior of Cu centers of enzymes, the electrochemical metallization of thin organic films with Cu, and the preparation of complex three-dimensional supramolecular Cu-containing structures with spatial order.

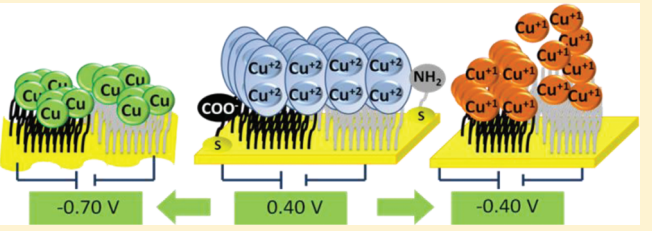

1. INTRODUCTION

Transition-metal complexes are promising candidates for modifying solid substrates due to the many possibilities of changing, in a controlled way, the physical and chemical properties of the substrate using extremely low amounts of material. Possible technological applications of transition-metal complexes immobilized on conducting surfaces by using polymers,[1] hydrogels,[2] or self-assembled monolayers[3] as structural matrixes are in the field of sensors, biosensors, catalysis, biocatalysis, and spintronics, among many others. Self-assembled monolayers (SAMs) have clear advantages over the other matrixes because their thickness can easily be adjusted at the nanometer level, while the spatial localization of metallic complexes can precisely be controlled by the terminal group of the SAM.[4]

The strategies used to immobilize metallic complexes on SAMs involve different types of interactions, namely, nonspecific adsorption, covalent bonding, and specific adsorption. Nonspecific adsorption on thiol-covered metallic surfaces involves electrostatic and hydrophobic interactions. This strategy has a variety of advantages: it is simple, fast, direct, and reversible. The disadvantages are easy desorption by a change of ionic strength, pH, or surfactants and random orientation of the molecules. The covalent coupling route is attractive in terms of good stability and high binding strength, while disadvantages involve random orientation, slow kinetics, difficult removal of reactants and side products, and the irreversible character of the bond.[5] Finally, specific interactions refer to a characteristic that is unique to a couple of binding partners, i.e., to the selectivity of the process where the interaction with an analyte or guest to form a supramolecular unit is an essential step. Coordination chemistry can be included in this last classification. The advantages of this strategy are improved orientation of the immobilized species, high specificity and functionality, and well-controlled and reversible adsorption. All these strategies have been used to immobilize different metallic complexes on thiol SAMs on metal surfaces.

Received: April 10, 2011
Revised: October 10, 2011
Published: November 03, 2011

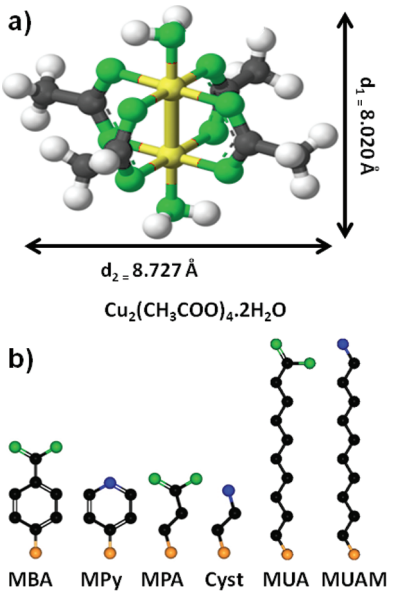

Figure 1. (a) Structure of the copper acetate complex: yellow, Cu; green, O; black, C; white, H. The Cu−Cu distance is 2.619 Å. (b) Different thiols used to immobilize the Cu complex on the Au(111) surface: orange, S; black, C; green, O; blue, N (H not shown).

Since Bleaney and Bowers discovered intramolecular antiferromagnetic interactions in binuclear copper acetate monohydrate,[6] this metallic complex has attracted considerable attention. In fact, binuclear copper(II) compounds are of particular interest due to their magnetic superexchange interactions between the copper atoms through the bridging ligands and also due to their remarkable stability. The coordination chemistry of Cu is particularly interesting because of its geometry, flexible redox properties, and variety of oxidation states. Coordination compounds have been known to be useful for constructing molecular information processing systems, particularly by biological self-organizing processes.[7−10] Copper acetate complexes immobilized on a mercaptohexadecanoic SAM on Au(111) have been used to build metal organic frameworks.[11] On the other hand, metal complexes have also been widely used to mimic the redox centers of metalloenzymes.[12] In the particular case of copper complexes, they have been taken as model systems[13] of Cu ion sites in different cuproproteins such as azurine,[14] nitrite reductase,[15] and laccase.[16] In addition, copper ions also have a wide variety of biological activities against bacteria[17] and fungi.[18]

Copper complexes have been used as a source of Cu(II) in inorganic synthesis and as a catalyst or as an oxidizing agent in organic reactions. In fact, binuclear copper(II) complexes have also been studied in relation to the catalysis of hydrogen peroxide reduction.[19] Very recently, scanning electrochemical microscopy (SECM) has been used to pattern an azido-functionalized glass substrate with a fluorescent dye molecule by click chemistry.[20] The Cu(I) catalyst required for this reaction was produced locally by reducing Cu(II) complexes by the SECM probe. Also copper complexes could be used to metallize thiol SAMs by electroreduction, as has been previously done for palladium on 4-mercaptopyridine SAMs on Au where the key issue seems to be the absence of metal ions in solution.[21]

Coordination chemistry combined with thiol SAMs constitutes an attractive strategy to immobilize copper acetate complexes to metal surfaces in a simple one-step method.[11,22] However, there are some basic questions that should be answered to use this strategy in the wide range of applications described above: (i) Which are the more efficient donors (chemical functionalities) to immobilize the Cu complexes on the SAMs? (ii) What fraction of the total donors (thiol molecules) in the SAM are involved in the immobilization process? (iii) How does the aromatic or aliphatic character of the SAM backbone affect the charge-transfer process from the Cu ionic species to the Au surface? (iv) What is the influence of the thiol size (SAM thickness) on this process? (v) Is it possible to reduce the Cu(II) ions to Cu(I), and then to Cu(0) preserving thiol SAM integrity? (vi) Are the Cu complexes also immobilized by methyl-terminated SAMs by penetration through SAM defects?

In this investigation we have studied the immobilization of $Cu_2(CH_3COO)_4 \cdot 2H_2O$ (hereafter CuAc) (Figure 1a) through the specific interaction with the N and O donors present at the terminal group of different aliphatic and aromatic thiol (Figure 1b) SAMs on Au(111). We have determined the efficiency of the different donors in immobilizing the CuAc complex, its spatial orientation, the presence of other species bound to the SAMs resulting from the dissociation of the complex, and the influence of the thiol backbone and hydrocarbon chain length on the Cu(II)/Cu(I) to Au(111) charge-transfer process. On the other hand, when these SAMs are prepared on nanostructured Au (NSAu), the Cu(I)/Cu(0) electrochemical process is also detected due to the enhanced stability of the thiol SAMs on this substrate against reductive desorption.[23] SERS measurements show that it is possible to spatially localize, with micrometer precision, the copper ionic species immobilized on SAMs of mixed thiols with different capturing abilities. Enhanced Cu ion capture and delivery was observed when NSAu was used as the substrate.

2. EXPERIMENTAL SECTION

2.1. Preferentially Oriented Au(111) Substrates and Chemicals. Vapor-deposited Au films (250 ± 50 nm in thickness) on a thin Cr layer supported on glass were used as substrates (Arrandee). They were annealed for 5 min in a butane−propane flame until the film color turned to dark red. After the thermal treatment, the polycrystalline substrates exhibit large grains with atomically smooth (111) terraces separated by steps of monatomic height. These preferentially oriented Au(111) substrates have been extensively used for the preparation of ordered SAMs because they exhibit the same coverage and structural characteristics as those formed in Au(111) single-crystal faces.[4,5,11,24,25] All the chemicals used were of analytical reagent grade. The different thiols, 4-mercaptobenzoic acid (MBA), 4-mercaptopyridine (MPy), cysteamine (Cyst), 11-mercaptoundecylamine (MUAM), 3-mercaptopropionic acid (MPA), 11-mercaptoundecanoic acid (MUA), and hexanethiol (HT), were used as received (Aldrich Chemical Co., Milwaukee, WI). $Cu_2(CH_3COO)_4 \cdot 2H_2O$ was Merck pa grade. Absolute ethanol and Milli-Q water were employed as solvents for the solutions.

2.2. NSAu Substrates. The NSAu substrates were prepared from polycrystalline Au foils following the procedure described by Arvia et al.[26] They were first cleaned with piranha solution, rinsed with Milli-Q water, and introduced into a conventional three-electrode glass cell using a saturated calomel electrode (SCE) and a high-area Pt foil as the reference and counter electrodes, respectively. The polycrystalline Au foil substrates were then anodized in 0.5 M H_2SO_4 solution for 15 min at 2.40 V (vs SCE) to form a thick hydrous gold oxide layer. Immediately

afterward, the hydrous oxide was electroreduced to metallic Au by applying a potential sweep from +2.40 to −0.60 at 0.025 V s^{-1}. The electrode was maintained at the final potential for 7 min to ensure the total electroreduction of the thick oxide layer.

As follows from scanning electron microscopy (SEM) images of the overlayer cross-section and scanning tunneling microscopy (STM) images of the surface, the nanostructured material is "black metallic gold" consisting of a columnar structure with a 10−20 nm diameter and a 400−500 nm length, separated by a large density of pores.[26−28] Ellipsometric data show that the density of the electrochemically prepared NSAu is ∼1/2 the density of bulk Au.[29] Monoenergetic positron beam results point out that a strong positron trapping by defects exists as a consequence of the large amount of pores in the columnar structure.[30] There is a distribution of open volumes with typical sizes that change along all the substrate thickness. STM images of these substrates are shown in the Supporting Information.

The real surface area (A) of the NSAu (after the anodization/reduction procedure) was estimated in the same electrolyte (0.5 M H_2SO_4 solution) by measuring the charge (Q) involved in the electroreduction current peak of the gold oxide monolayer recorded after applying a triangular potential scan from −0.25 to +1.60 V at v = 0.1 V s^{-1} to the NSAu. The A value was then calculated as $A = Q/q_{mon}$, where q_{mon} is the charge density related to the electroreduction of a gold oxide monolayer (q_{mon} = 0.44 mC cm^{-2}). Typical A values used in this work were 15−50 cm^2. After the estimation of A, the electrodes were removed from the acid solution, rinsed with NaOH, water, and ethanol, and immersed in the thiol-containing solutions. As recently reported, alkanethiolate monolayers stabilize the NSAu by reducing the surface mobility, thus avoiding surface area decay.[31]

2.3. Self-Assembly of Alkanethiols and Aromatic Thiols on Au. Thiol SAMs were prepared by immersing the Au substrates (preferentially oriented Au(111) or NSAu) in freshly prepared thiol-containing solutions at room temperature in the absence of light. For each thiol, different solvents, incubation times, and concentrations were tested. The best conditions to obtain optimal thiol coverage (estimated by reductive desorption and X-ray photoelectron spectroscopy (XPS)) were as follows: Cyst, 1 mM aqueous solution, 1 h; MPy, 1 mM aqueous solution, 5 min; MUAM, 1 mM ethanolic solution, 24 h; MPA, 1 mM aqueous solution, 1 h; MBA, 1 mM ethanolic solution, 30 min; MUA, 1 mM ethanolic solution, 24 h. Control experiments were also made using HT SAMs prepared in 1 mM ethanolic solution for 24 h. Finally, a vigorous rinsing was done with the corresponding solvents before drying under N_2. The conditions to form complete SAMs were the same in both Au(111) and NSAu substrates as has been shown by electroreductive desorption experiments.[23,31]

2.4. Copper Acetate Immobilization. The CuAc was immobilized by immersing the SAM-covered Au(111) substrate in 1 mM aqueous CuAc solution for 1 h at room temperature in the absence of light. In fact, it has been shown that light could affect the SAM integrity.[23] Longer immersion times did not increase the amount of immobilized Cu species. Afterward, the samples were repeatedly rinsed with water and dried under a N_2 flow. For the NSAu substrate the immersion time was 12 h to allow the filling of the porous structure with the copper complex.

A second CuAc layer was also immobilized on a CuAc−MBA SAM−Au(111) structure by using 4,4′-bipyridine (BiPy) as the linker. After the first CuAc layer had been prepared and characterized, the sample was immersed in 1 mM ethanolic bipyridine solution for 12 h. The substrate was then vigorously rinsed with ethanol, and afterward a second immersion in 1 mM aqueous CuAc solution for 2 h was done to form the second CuAc layer.

2.5. Electrochemical Measurements. Electrochemical runs were performed with a TEQ-potentiostat with data acquisition capabilities. The Au substrates were mounted in a conventional three-electrode glass cell using an SCE and a high-area platinum foil as the reference and counter electrodes, respectively. Solutions were degassed with nitrogen prior to the experiments. All potentials were measured and reported with respect to the SCE reference electrode.

Triangular potential scans from −0.4 to +0.4/0.5 at 0.05 V s^{-1} were applied to the Au substrates with the CuAc immobilized in the SAMs in deaerated aqueous 0.1 M phosphate buffer (pH 7.4). The amount of electrochemically active CuAc was estimated from the charge density involved in the anodic peak of the Cu(II)/Cu(I) redox couple.

Reductive desorption of thiols from the Au substrates, with and without immobilized CuAc species, was performed from +0.55 to −0.85 at 0.05 V s^{-1} for SAMs on Au(111) and from +0.55 to −1.4 at 0.05 V s^{-1} for SAMs on NSAu substrates in deaerated aqueous 0.5 M phosphate buffer (pH 7.4) at room temperature. The charge density and the peak potential involved in the reductive desorption process were taken as an estimation of the SAM surface coverage and SAM stability, respectively. Further details on charge density calculations have been reported in a previous publication.[32]

2.6. X-ray Photoelectron Spectroscopy (XPS) Measurements. XPS was performed using a Mg Kα source (XR50, Specs GmbH) and a hemispherical electron energy analyzer (PHOIBOS 100, Specs GmbH) with an electron takeoff angle of 90°. A two-point calibration of the energy scale was performed using sputtered cleaned gold (Au $4f_{7/2}$, binding energy (BE) = 84.00 eV) and copper (Cu $2p_{3/2}$, BE = 932.67 eV) samples. For the deconvolution of the S 2p and Au 4f spectral regions, a Shirley-type background was subtracted, and a combination of Lorentzian and Gaussian functions was used. In the case of S 2p, the full width at half-maximum (fwhm) was fixed at 1.1 eV and the spin−orbit doublet separation of the S $2p_{3/2}$ and S $2p_{1/2}$ signals was set to 1.2 eV. The BEs and peak areas were optimized to achieve the best fit. For the Au 4f region, the fwhm of the peaks was 1.0 eV, and the spin−orbit doublet separation of Au $4f_{5/2}$ and Au $4f_{7/2}$ was set to 3.65 eV. The S/Au ratio was estimated by the measurement of the peak area of Au 4f and S 2p signals corrected by the relative sensitivity factor of the elements. The settings for the C 1s region were left free to quantify the O—C═O species. For all samples the intensity in the C 1s region with a maximum at 288.9−289.2 eV was assigned to the O—C═O species.[33]

The surface coverage by the thiol molecules was estimated from the thiolate S 2p (162 eV)/Au 4f intensity ratio using as a reference the value corresponding to hexanethiol, which has a surface coverage θ_{SAM} = 0.33.[4] In this case the photoelectron attenuation factors introduced by the presence of the organic layer are similar for S and Au, and the attenuation factor from Au due to the S atom contribution is negligible. On the other hand, the CuAc surface coverage on the thiol SAM was estimated from the Cu 2p/S 2p (162 eV) intensity ratio. In this case we have used the attenuation factor in monolayers of n-alkanethiols already described in the literature.[34]

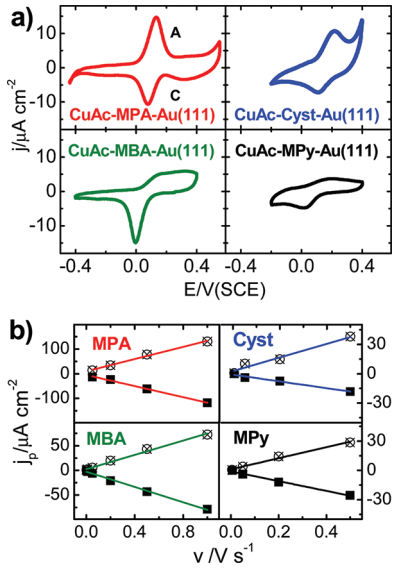

Figure 2. (a) j vs E profiles for the immobilized Cu(II)/Cu(I) redox couple (first scan) on different thiol SAMs on Au(111) recorded when a triangular potential scan at 0.05 V s^{-1} in deaerated aqueous 0.5 M phosphate buffer (pH 7.4) at room temperature is applied. (b) j_p vs v plot for the Cu(II)/Cu(I) redox couple on different thiol SAMs on Au(111).

Table 1. Electrochemical Data for CuAc Immobilized on Different SAMs on Au(111)[a]

thiol	ΔE_p/V vs SCE	q_{des} / μC cm^{-2}	E_p^D(thiol)/V vs SCE	E_p^D(thiol + CuAc)/V vs SCE
MBA	0.10−0.12	55 ± 5	−0.61	−0.63
MPA	0.06	65 ± 10	−0.57	−0.56
MUA	0.20	*b*	−0.89	−0.94
MPy	0.10−0.12	58 ± 6	−0.76	−0.77
Cyst	0.07−0.20	60 ± 6	−0.61	−0.76
MUAM	0.20	*b*	−0.87	−0.89

[a] Column 2: separation between the anodic and cathodic peaks for the Cu(II)/Cu(I) redox couple immobilized on different CuAc−thiol SAMs−Au(111). Column 3: thiol reductive desorption charge densities for either plain thiol SAMs or CuAc−thiol SAMs−Au (111). Column 4: thiol reductive desorption peak potentials for plain thiol SAMs−Au(111). Column 5: thiol reductive desorption peak potentials for CuAc-thiol SAMs−Au(111). [b] An estimation of q_{des} is not given because the electrodesorption peaks of MUA and MUAM SAMs are partially superimposed to the hydrogen evolution reaction.

2.7. Surface-Enhanced Raman Spectroscopy (SERS). The Raman scattering experiments were performed on NSAu substrates modified with a mixed MBA and HT SAM on which the CuAc complex was then immobilized. A Jobin-Yvon T64000 triple spectrometer, operating in subtractive mode and equipped with a liquid N_2 cooled charge-coupled device (CCD) and a confocal microscope (Olympus BX41) with a 10× long working distance objective, was used. Maps were typically 100 × 100 μm^2 in size (5 μm step) with 30 and 45 s integration times for the MBA and CuAc spectral regions, respectively. The excitation was done using the 647.1 nm line of an Ar−Kr laser and 40 mW of laser power.

3. RESULTS AND DISCUSSION

3.1. Electrochemical Characterization. Figure 2a shows the current density (j) vs potential (E) profiles for MPA, MBA, Cyst, and MPy SAM-covered Au(111) recorded at 0.05 V s^{-1} in deaerated aqueous 0.5 M phosphate buffer (pH 7.4) after substrate immersion in the CuAc-containing solution for 1 h followed by careful rinsing. In all cases j vs E profiles show a cathodic peak related to the Cu(II) to Cu(I) electroreduction (peak C at 0.0/0.1 V) and a broader anodic region (peak A at 0.0/0.3 V) related to the Cu(I) to Cu(II) electro-oxidation reaction. The presence of the Cu(II)/Cu(I) redox couple is a clear indication that CuAc species have been immobilized on the thiol SAMs and that they are able to participate in the charge-transfer process with the Au substrate. However, for MUA and MUAM the Cu(II)/Cu(I) redox couple is too small, so that it is hardly visible in the double-layer region of the SAM-covered Au (see the Supporting Information).[16] It should be noted that blank experiments made using a methyl-terminated SAM (hexanethiol) show no traces of the Cu(II)/Cu(I) redox couple (see the Supporting Information), which points out the key role of the terminal group in immobilizing the complex.

The plot of maximum anodic (j_{pa}) and cathodic (j_{pc}) peak current density vs scan rate (v) for the Cu(II)/Cu(I) redox couples yields straight lines typical of a surface-controlled electrochemical reaction, irrespective of the SAMs where the CuAc is immobilized (Figure 2b). The separation between the anodic and cathodic peaks (ΔE_p) and its dependence on v gives information about the charge-transfer process (Table 1). For an ideally reversible behavior of the adsorbed species, ΔE_p should be zero and independent of the v value. However, most of the nearly reversible redox systems experimentally reported are, indeed, characterized by finite values of ΔE_p.[35] Our results for the ΔE_p vs v dependence for the CuAc immobilized on MPA, MBA, and MPy SAMs indicate that ΔE_p is nearly independent of v in the 0.005 V < v < 1 V range. However, the magnitude of the ΔE_p value depends strongly on the thiol SAM: $\Delta E_p \approx 0.060$ V for MPA and $\Delta E_p \approx 0.10-0.12$ V for MBA and MPy. On the other hand, for the Cu species immobilized on Cyst, ΔE_p changes from 0.07 to 0.20 V as v increases from 0.005 to 0.20 V s^{-1}. The more irreversible behavior evidenced at higher sweep rates for the Cu(II)/Cu(I) couple on cysteine SAMs has been reported previously.[36] Finally, for the Cu complex immobilized on MUA and MUAM, $\Delta E_p \approx 0.20$ V for $v = 0.05$ V s^{-1}. As we have mentioned before, the charge involved in MUA and MUAM SAMs is too small to be estimated, but ΔE_p can be determined in both cases from small shoulders in the double layer. The low ΔE_p value and its independence on v for the CuAc immobilized on MPA suggest the presence of an almost reversible surface-bound redox system, whereas a more irreversible behavior is observed for these species immobilized on the other SAMs, in particular for the long MUA and MUAM thiols, in agreement with previous observations on redox couples immobilized on different SAMs.[37]

Another interesting observation is the broad shape of the current peaks (in particular the anodic one) related to the Cu(II)/Cu(I) redox couple as shown in Figure 2a. We observe that in some cases the anodic peak splits into a doublet, a fact that could be due to the two different Cu(II) ions present in CuAc (Figure 1a). In general, the j vs E shape for surface-controlled redox processes depends on different factors such as the lateral interactions, the coverage of the immobilized species, and the distribution of formal potentials of the redox centers due to

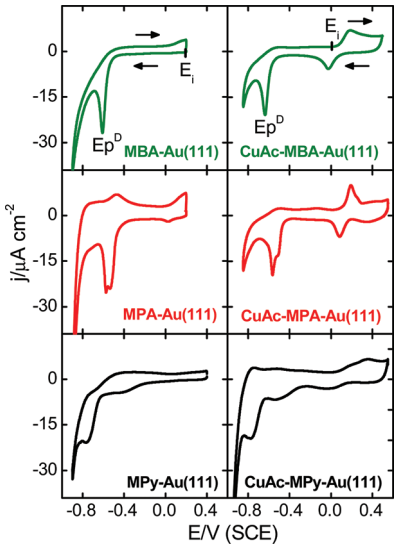

Figure 3. j vs E profiles recorded at $\nu = 0.05$ V s^{-1} for thiol SAMs on Au(111) (left panel) and CuAc−thiol SAM−Au(111) surfaces (right panel) in deaerated aqueous 0.5 M phosphate buffer (pH 7.4) at room temperature. The potential at which the electrochemical run is initiated (E_i), the reductive desorption peak potential (E_p^D), and the scan direction (arrows) are indicated.

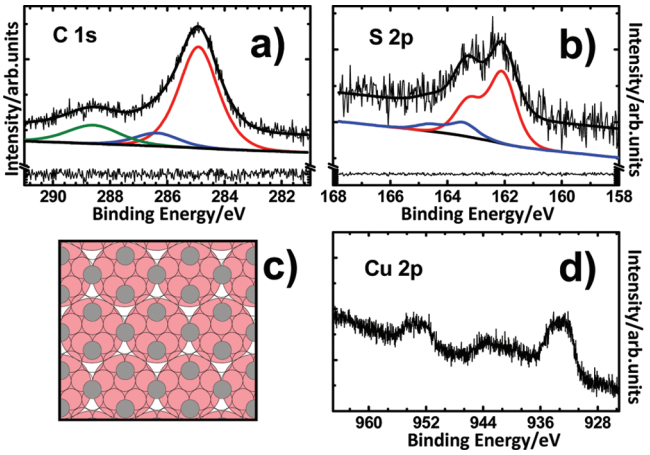

Figure 4. (a) C 1s and (b) S 2p XPS regions and residual data analysis for CuAc−MUAM SAM−Au(111). The fitting parameters for the region C 1s were left free to quantify O—C═O species. For all samples the intensity in the C 1s region with a maximum at 288.9−289.2 eV (green line) was assigned to O—C═O species. S 2p region components were assigned to thiolate (red) and unbound thiol (blue). (c) Scheme showing a close-packed array of CuAc (pink) on a $\sqrt{3}\times\sqrt{3}$ $R30°$ thiol lattice (gray). (d) The Cu 2p region presents shakeup peaks indicating the presence of Cu(II).

different environments existing at the interface, among others.[38,39] In the case of SAMs there is also a distribution of electron-transfer rates due to variations in the molecular environment of the redox center caused by SAM defects.[40] In particular, for ideal reversible electrochemical behavior, the peak width fwhm for a one-electron process should be 90.6 mV at 25 °C. A value of fwhm of 0.20 V for surface-grafted copper(II) benzoate complexes has been assigned to the dispersion of redox potentials resulting from the different environments existing at the interface.[41] Thus, the different shapes of the j vs E profiles for the Cu(II)/Cu(I) redox couple could result from the different order and/or environments existing at the different SAMs.

Further analysis regarding the charge-transfer process is presented in section 3.3 after evaluation of the SAM and CuAc surface coverage by a complementary technique (XPS).

Interesting conclusions can be obtained by comparing the reductive desorption curves of thiol- and CuAc-modified SAMs (Figure 3). In all cases the j vs E profiles show thiol desorption peaks at a potential (E_p^D) preceding the hydrogen evolution reaction. Also for the CuAc−SAM−Au(111) systems the Cu(II)/Cu(I) redox couple is always clearly visible in the j vs E profiles (Figure 3, right panel). The electroreductive curves for CuAc−thiol SAMs show some broadening and lower current peak maxima. Thus, charge involved in the desorption peak (q_{des}) is slightly lower (between 5% and 10%) than those obtained for the nonmodified SAMs. For this reason the q_{des} value for each surface has been taken into account to estimate the immobilization efficiency of the complex.

A dense alkanethiol SAM in $\sqrt{3}\times\sqrt{3}$ $R30°$ or $c(4\times2)$ involves 75 μC cm^{-2}.[32] We found $q_{des} = 55/60 \pm 10$ μC cm^{-2} for short thiols such as MPA,[42,43] MBA,[44] Cyst,[45,46] and MPy[47,48] for which SAMs containing domains of diluted surface structures have been described. Although q_{des} gives a reasonable estimation of the SAM surface coverage, one should be aware that it could involve errors of about 10%.[49−52]

For MUA and MUAM SAMs on Au similar thiol desorption peaks are observed, irrespective of the presence or absence of immobilized CuAc species. However, in these cases an estimation of q_{des} is difficult because these peaks are partially superimposed on the hydrogen evolution reaction at pH 7. The fact that no significant differences in the reductive desorption behavior were observed between SAMs with and without the immobilized species suggests that no displacement of thiol molecules by the CuAc complexes takes place.

3.2. XPS Characterization. XPS was used to estimate the SAM coverage and also to measure the total amount of Cu(II) species bonded to the SAM−Au(111) surface. This value can be compared with the amount of electrochemically active Cu(II) detected by the triangular potential scans (Figure 2). In Figure 4 typical XPS spectra for the C 1s (a), S 2p (b), and Cu 2p (d) regions and residual data analysis for CuAc−MUAM SAM−Au(111) are shown. The S 2p signal was fitted with a major component at 162 eV (red line) and a small one at 163 eV (blue line) that correspond to thiolate and some amount of free thiol, respectively.[4] On the other hand, for the C 1s signal the green line can be assigned to the contribution of the carboxyl groups.[33,53] The Cu 2p region presents a broad peak at 933.4 eV and shakeup satellites at 942.5 eV. These features are characteristic of Cu(II).[54] The results for the different thiols are summarized in Table 2.

First, we analyze the thiol SAM surface coverage (θ_{SAM}) measured by XPS using the thiolate 162 eV component of the S 2p signal. For a dense alkanethiol SAM such as hexanethiol (used as a control SAM in this work), the SAM surface coverage is θ_{SAM} =0.33.[4] Taking this value as a reference, we determined all SAM surface coverages from the S (162 eV)/Au 4f ratio. In the case of the long MUA and MUAM, we obtained θ_{SAM} = 0.28 (Table 2), a value somewhat lower than that found for complete SAMs in a standing-up configuration [$\sqrt{3}\times\sqrt{3}$ $R30°$ or $c(4\times2)$].[4] In fact, it has been reported that SAMs of long amine-terminated thiols have a lower S 2p XPS signal than that expected

Table 2. XPS and Electrochemical Data for the CuAc Immobilized on Different SAMs on Au(111)[a]

thiol	θ_{SAM}	Cu/S ratio	$q_{Cu}/\mu C\ cm^{-2}$
MBA	0.24	0.20 (0.48)	15.5 (36)
MPA	0.28	0.17 (0.56)	19.5 (42)
MUA	0.28	0.24 (0.56)	1.5 (42)
MPy	0.21	0.11 (0.42)	6.3 (31)
Cyst	0.23	0.26 (0.46)	14 (35)
MUAM	0.28	0.19 (0.56)	1.7 (42)

[a] Column 2: θ_{SAM} calculated from the S (162 eV)/Au signal ratio. Column 3: Cu/S ratio calculated from XPS data. The number in parentheses corresponds to the maximum Cu/S ratio for each SAM calculated from the experimental θ_{SAM} and the theoretical maximum value (2/3) for CuAc on the $\sqrt{3}\times\sqrt{3}$ $R30°$ thiol lattice. Column 4: maximum q_{Cu} for each SAM calculated from the j vs E profiles (Figure 2). The number in parentheses corresponds to the value of the maximum charge according to θ_{SAM}.

for a complete SAM.[55] In the case of MUA SAMs, some amount of lying-down molecules coexisting with the dense standing-up phase has also been detected by thermal desorption spectroscopy irrespective of the preparation conditions, a fact consistent with a smaller surface coverage.[56] On the other hand, the SAM surface coverage for Cyst, MBA, MPA, and MPy estimated from XPS (Table 2) is consistent with the presence of more complex surface structures than the usual $\sqrt{3}\times\sqrt{3}$ $R30°$ or $c(4\times2)$[4] lattices. In fact, in these SAMs it has been shown that diluted[44−48] and dense[32,57] domains of thiol molecules coexist. Considering that θ_{SAM} = 0.33 corresponds to q_{des} = 75 $\mu C\ cm^{-2}$, there is a reasonable agreement in the XPS coverage and the electrochemical data for these SAMs (Table 1) taking into account the 10% error involved in surface coverage estimation from reductive desorption experiments.[49−52]

The Cu/S relationship gives a direct measure of the CuAc complex surface coverage (θ_{CuAc}), which in the following is always defined in relation to the underlying thiol SAM. Let us consider a compact array of CuAc on a dense thiol SAM (θ_{SAM} = 0.33). Taking into account the CuAc molecular size[58] (see Figure 1a), one obtains θ_{CuAc} = 1/3 (Figure 4c). As the complex has two Cu ions per molecule, the Cu/S ratio in the XPS data for a complete CuAc monolayer on a dense thiol SAM should be θ_{Cu} = 2/3. However, for an estimation of the maximum amount of CuAc expected per thiol molecule, one should consider the real (experimental) θ_{SAM} because it determines the number of coordination sites available for CuAc immobilization. Table 2 shows that all systems exhibit θ_{Cu} values ranging between 26% (for MPy) and 56% (for Cyst) of the maximum Cu/S ratio expected for the SAMs studied in this work.

The COO/Cu ratio in CuAc is 2/1 (see Figure 1), thus, it could give information about the how the CuAc complex binds the SAM. First, we analyze the CuAc binding to COO-terminated SAMs. If the CuAc complex was able to bind the COO-terminated SAM by displacement of the axial water molecule, this ratio should have been 3.5. On the other hand, if this binding takes place by displacement of one COO ligand by the terminal COO group of the SAM, the ratio should be 3.0. This ligand exchange mechanism has been recently reported for acetate−Ru complexes immobilized on COOH-terminated SAMs.[59] Despite the scatter in determining the COO component in the C 1s XPS signal, the COO/Cu ratio is ∼3.2. Thus, we cannot decide how the complex is bonded to the terminal COO groups: both contributions are possible. On the other hand, one should consider the extra contribution of free Cu(II) ions arising from the CuAc dissociation that can also be efficiently immobilized by the COOH terminal groups of the SAM. This is reasonable since the stability constant of the complex[60] is $K_s \approx 1000$, and COOH-terminated SAMs on Au are able to detect about 1 ppq (parts per quadrillion) Cu(II) ions.[43,61] However, significant Cu(II) anchoring from the CuAc dissociation by simple electrostatic interactions should result in significantly lower COO/Cu ratios (approaching 1) than that experimentally measured so that this contribution should not be the most important in our system.

Now we turn to the CuAc binding to N-terminated SAMs. In this case the experimental COO/Cu ratio is ∼5.8, while for axial water molecule displacement the expected ratio should be 2. In this case water displacement could be the main mechanism operating in these SAMs because ligand displacement should reduce the amount of COO in relation to Cu, leading to values smaller than 2. The excess of COO can be explained considering free COO ions in equilibrium with the CuAc complex that can be incorporated since it is known that acetate ions are able to interact with pyridine and amine-terminated thiols.[62,63]

3.3. Electrochemically Active CuAc Immobilized on Different SAMs. The maximum charge for the Cu(II)/Cu(I) redox couple (q_{Cu}) expected for a close-packed array of CuAc immobilized on a thiol SAM with θ_{SAM} = 0.33 should be $q_{Cu} \approx 50$ $\mu C\ cm^{-2}$ (see Figure 4c). However, to estimate the real fraction of electrochemically active Cu(II) for each system, this figure should be referred to the real θ_{SAM} as shown in Table 2. Taking into account these considerations, we found that short thiols (SAM thickness h = 0.5 nm for MPA,[64] h = 0.78 nm for MBA,[65] and h = 0.48 nm for Cyst[66]) exhibit q_{Cu} values in the 14−19 $\mu C\ cm^{-2}$ range, which represents about 40−50% of their complete monolayer (Table 2), in fair agreement with the experimental amount of immobilized CuAc derived from the XPS data. This means that practically all immobilized Cu ions are electrochemically active. This is also true for MPy SAMs where we found a smaller CuAc surface coverage ($\theta_{Cu} \approx 1/4$), although almost all Cu ions participate in the charge-transfer process. On the other hand, the smallest q_{Cu} value is obtained for the thick MUA SAMs (h = 1.9 nm)[66] despite the fact that this thiol captures a large amount of Cu ions as shown by XPS data (Table 2). This result can be explained considering that, in this case, the immobilized CuAc is far from the Au substrate, and accordingly, the tunneling probability is relatively small. Therefore, only a small fraction (less than 5%) of the redox centers participate in the charge-transfer process. This is also in agreement with the data for MUAM SAMs (h = 1.75 nm),[67] where we found about 1/3 monolayer of the Cu complex by XPS, but only a small electrochemical activity is recovered (q_{Cu} =1.7 $\mu C\ cm^{-2}$, see the Supporting Information).

One can conclude that the best electrochemical efficiency is observed for SAMs of short thiols such as MPA, Cyst, MBA, and MPy. However, in the latter case the immobilization efficiency is lower than in the other short thiols, a fact that could be explained considering steric hindrance. In fact, it has been found that 4MPy molecules on Au(111) can adopt for ordered diluted phases with surface coverage close to 0.2 (as in the case of our measurements) configurations with tilt angles of ca. 60° from the surface normal,[68] which is higher than the 30° tilt angles of thiols in SAMs on Au(111). In those configurations the anchoring capability of MPy for the large CuAc (8.7Å × 8.0 Å) should be reduced

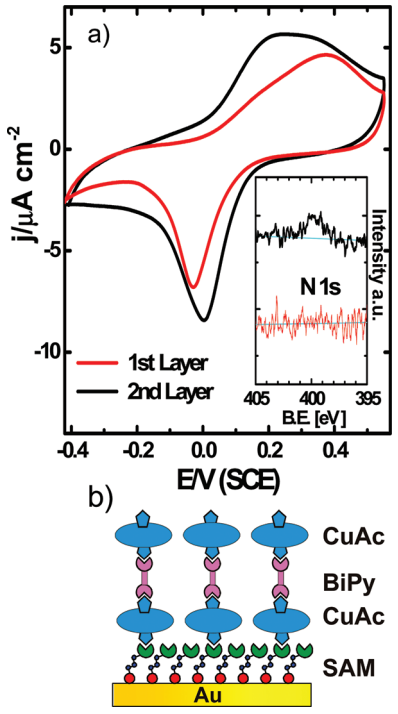

Figure 5. (a) j vs E response to a triangular potential sweep at $v = 0.05$ V s^{-1} of the Cu(I)/Cu(II) system in 0.5 M phosphate buffer (pH 7.4) at room temperature before (red curve) and after (black curve) CuAc immobilization on BiPy−CuAc−MBA SAM−Au(111). Inset: XPS N 1s signal after immobilization of BiPy on CuAc−MBA SAM−Au(111) (black curve) and without BiPy (red curve). (b) Scheme of the ideal supramolecular structure.

because the AcCu complex could shield a large number of MPy molecules or the specific interaction of the N of MPy and the complex would not be favored. Such a high tilt angle has not been reported in the literature for Cyst, MBA, and MPA.[69−71] The better electrochemical activity for the short thiols observed in our experiments agrees with that found for the Cu(II)/Cu(I) redox center of azurine immobilized on n-alkanethiol SAMs. In fact, in this case the electrochemical electron-transfer rate constant is almost independent of the chain length up to ca. 8−9 methylene units (n) but follows an exponential distance decay with a decay factor (β) of $(1.03 \pm 0.02)/n$ at longer chain lengths.[7273] Note also that we do not observe a significant difference in the charge-transfer behavior between the aromatic and aliphatic thiols used in this work, in agreement with previous results for thiol SAMs on Au in contact with different redox couples.[74] In fact, for short thiols direct tunneling from the Au surface to the redox center is expected. On the other hand, the resistance of n-alkanethiols increases exponentially with n along the tunneling pathway.[75] For that reason, the longest MUA and MUAM thiols are the worst linkers for electrochemical applications due to their low tunneling efficiency as the redox centers are far away from the Au surface. Finally, our results show that the charge-transfer process is mainly determined by the size of the thiol molecule with no influence of the nature of the spacer (aromatic or aliphatic) or the terminal group (N or O). However, it is evident that the O donors are more efficient for CuAc immobilization in the specific adsorption process.

3.4. Spatial Orientation of the CuAc Species on the SAMs. The spatial orientation of CuAc in the outer part of the SAMs was tested by binding BiPy molecules on top of the immobilized CuAc−MBA SAM−Au(111) structure (first layer). We have used MBA for the first layer because it combines a good efficiency for CuAc immobilization, good electron transfer from CuAc (see Table 2), and a more rigid structure (provided by the aromatic ring) to build the supramolecular structure than the aliphatic chains of short thiols such as Cyst and MPA. In addition, the MBA SAM configures an extended aromatic structure with bipyridine that could assist charge transfer through the copper ions of the complex. After immersion of the first layer in a solution containing BiPy followed by a vigorous rinsing, XPS data show a clear N 1s signal and an S/N ratio of 0.64 (inset in Figure 5a) indicating that BiPy molecules are able to interact with the layer of the immobilized complex. The BiPy-modified first layer was then immersed for 2 h in the CuAc-containing solution. Finally, the sample was thoroughly rinsed with water and transferred again to the electrochemical cell containing phosphate buffer to measure q_{Cu} from the j vs E profiles. Results from the electrochemical runs (Figure 5a) show that q_{Cu} increases ∼40% in going from the first (Table 2) to the second CuAc layer. The scheme of the ideal supramolecular structure CuAc−BiPy−CuAc−MBA SAM−Au(111) built by this procedure is shown in Figure 5b. The possibility that BiPy molecules were immobilized on noncoordinated carboxylates of the underlying MBA SAM was discarded by making control experiments where MBA SAM−Au(111) samples were immersed in BiPy solutions and then in CuAc. In this case the N 1s signal in the XPS spectrum was practically undetectable. These results indicate that this strategy can be used to build complex electrochemically active supramolecular structures.

It is important to note that the increase in q_{Cu} measured from the j vs E profiles corresponds to ∼6 μC cm^{-2}, i.e., a value that coincides with that measured for CuAc immobilized on MPy SAMs (both MPy and BiPy have a pyridine terminal group). In contrast to MUA and MUAM, where only a few Cu ions are electrochemically active, those linked to the BiPy molecules participate in the charge-transfer process, although they are placed more than 2 nm away from the Au surface. This result indicates that the BiPy molecules in the CuAc−BiPy−CuAc−MBA SAM−Au(111) supramolecular structure are able to electrically link the redox metallic centers of the first and second CuAc layers, allowing the charge transfer to the Au substrate, in contrast to the long aliphatic thiols.[75,76] In fact, it has been shown that the molecular conductance for a single BiPy molecule is 8 times greater than for a short aliphatic dithiol ($n = 6$).[75] Thus, in the case of long thiols such as MUA, penetration of the redox species through the SAM dominates electron transfer.[77]

Finally, it is interesting to note that in all cases we were unable to observe the Cu(I)/Cu(0) redox reaction in the j vs E profiles performed in the potential windows where SAMs are stable (see Figure 2). There are two possible reasons for this behavior: the SAMs completely block the second electron transfer of the Cu(II) ion, or the SAMs are desorbed before the Cu(I) reduction to Cu(0). In section 3.5 we study this point by using NSAu substrates. These substrates exhibit greater electrochemical and chemical stability for thiols,[23] and the amount of Cu(II) immobilized by the SAM-covered Au surface should be largely increased due to their large surface area. In addition, the shift in the electrodesorption potential of thiols toward more negative values than on Au(111) and a large electrochemical current could allow the detection of the Cu(I)/Cu(0) redox process on the intact SAM, thus providing a method for SAM metallization.

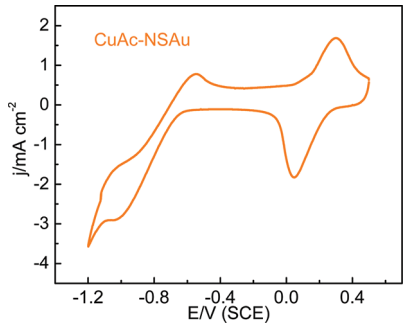

Figure 6. j vs E recorded at $v = 0.05$ V s^{-1} for CuAc adsorbed on NSAu in 0.5 M phosphate buffer (pH 7.4) at room temperature.

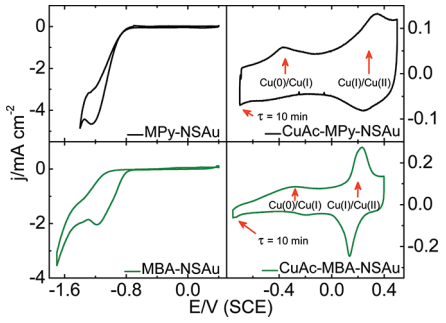

Figure 7. Reductive desorption curves recorded at $v = 0.05$ V s^{-1} for thiol SAMs on NSAu (left panel) and triangular potential scan at $v = 0.05$ V s^{-1} for the immobilized Cu(I)/Cu(0) and Cu(II)/Cu(I) redox couples (first scan) for CuAc−thiol SAM−NSAu surfaces (right panel) in 0.5 M phosphate buffer (pH 7.4) at room temperature. The holding time (τ) at the cathodic limit was 10 min.

3.5. CuAc Immobilization on Thiol SAM-Nanostructured Gold. In Figure 6 the j vs E profile for CuAc immobilized on the SAM-free NSAu in phosphate buffer is shown. The j vs E profile exhibits the well-defined Cu(II)/Cu(I) couple at 0.3/0.05 V previously discussed and a more irreversible process related to the Cu(I)/Cu(0) electrochemical reaction with anodic and cathodic waves located at −0.6 and −1.0 V, respectively, overlapping the hydrogen evolution reaction (HER). Three aspects can be highlighted from Figure 6. The first one is that the anodic charge related to the Cu(I)/Cu(0) redox reaction is smaller than the cathodic one due to the contribution of the HER in the cathodic wave. Second, the charge involved in the Cu(0)/Cu(I) process is lower than that of Cu(I)/Cu(II) because, in the potential window scanned (limited to the stability of the solvent), only a fraction of the total amount of Cu(I) species can be reduced to Cu(0). Finally, and important to note, is that the Cu(I) to Cu(0) process starts at −0.65 V, which is in the same potential range where thiol desorption on Au(111) takes place (Figure 3).

Interestingly, the j vs E profiles corresponding to MPy and MBA on the NSAu substrates show thiol electrodesorption peaks at ∼−1.2 V (Figure 7a,c); i.e., the stability range of the SAMs on this substrate has been markedly extended in relation to that observed on the Au(111) surface. The extended SAM stability window on NSAu allows the possibility of SAM metallization by reduction of the Cu(II) ions present in the CuAc complex to Cu(0). To test this possibility, MPy SAMs on NSAu and MBA SAMs on NSAu were immersed in the CuAc-containing solution to immobilize the CuAc species, thoroughly rinsed with water, and then polarized at −0.70 and −0.75 V for MPy and MBA, respectively, in the plain buffer solution for 10 min (Figure 7b,d). At this potential no desorption of MPy and MBA takes place (Figure 7a,c), but a certain amount of Cu(I) should be reduced to Cu(0) (Figure 6). In fact, after the CuAc−MPy SAM−NSAu substrate sample is held at −0.70 V for 10 min, a clear signal corresponding to the Cu(0) to Cu(I) electro-oxidation reaction can be observed in the anodic scan preceding the Cu(I) to Cu(II) reaction (Figure 7b). Thus, in principle, this electrochemical procedure could be used for Cu metallization of thiol SAMs on NSAu. In particular, the use of the CuAc complex, as the source of Cu(II) ions for the metallization, is attractive because its size could hinder penetration through SAM defects.[78]

However, the amount of Cu(I) species detected in the anodic scan is considerably lower than that involved in the Cu(I)/Cu(II) redox couple. Evidently, at this potential and holding time only a small fraction of the total amount of Cu(I) species formed in the first reduction wave (Cu(II) to Cu(I) reaction) can be reduced to Cu(0), as is also concluded from the analysis of Figure 6 for the SAM-free CuAc electroreduction on NSAu substrates. Note that the holding potential was selected as the more negative value at which metallization takes places on these substrates (Figure 6) but preserving the SAM integrity (Figure 7a,c).

On the other hand, from the point of view of Cu(II) capture, the NSAu substrates are interesting platforms for ion sensing. In fact, the comparison between Figure 7 and Figures 2 and 3 indicates that the amount of charge involved in the Cu(I)/Cu(II) redox couple increases by a factor ∼30 when the NSAu substrates are used.

Also these substrates allow us to perform SERS measurements to spatially localize, with micrometer precision, Cu ion-rich regions on SAMs of mixed thiols with different capturing abilities. XPS spectra and electrochemical results of HT SAMs on Au after immersion in CuAc demonstrated that this thiol is not able to immobilize the CuAc complex. Therefore, we have immobilized the CuAc complex on a mixed MBA and HT SAM on NSAu to test the spatial order correlation of the CuAc complex with the MBA domains by SERS. The aim was to highlight the importance of the SAM terminal group in the immobilization process. NSAu being a surface-enhanced Raman scattering active substrate, we performed micro-Raman maps to detect both the MBA and the CuAc complex spatial distributions (parts b and c, respectively, of Figure 8) in the same sample region. To avoid spectral congestion problems related to the presence of three different species (MBA, HT, and CuAc) in the sample, we selected different spectral regions to be followed and, in that way, unambiguously identified each one of them. For MBA we follow the 1590 cm^{-1} strong band, which mainly dominates the MBA SERS spectra and has been assigned to the ν_{8a} aromatic ring vibration mode[79] (Figure 8a). In the CuAc case we follow the 300 cm^{-1} region, where five different bands have been reported: δ(O−Cu−O) = 223 and 234 cm^{-1}, δ(Cu−Cu−O$_w$) = 254 cm^{-1} (O$_w$ being an oxygen atom from a water ligand), ν(Cu−O$_w$) = 302 cm^{-1}, and ν(Cu−O) = 323 cm^{-1}.[80] As a result, a broad band is clearly observed, and it can only be assigned to an overlap of all CuAc modes (Figure 8d).

The spatial correlation between the O donor SAM (MBA) and the CuAc complex becomes evident when we look at the corresponding 100 × 100 μm^2 SERS maps presented in Figure 8b,c. There are regions where both MBA and CuAc are detected, and

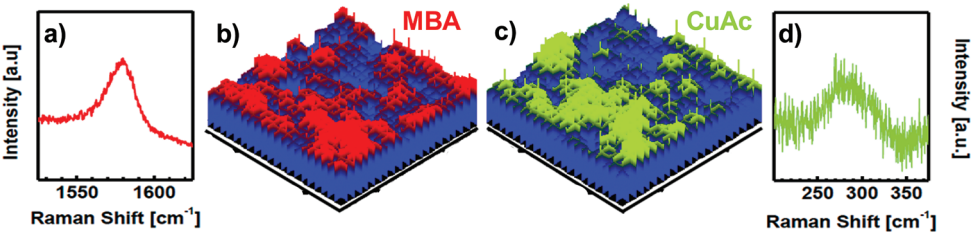

Figure 8. (a) MBA 1590 cm^{-1} ν_{8a} aromatic ring vibration mode, (b) 100 × 100 μm^2 SERS map following the spatial distribution of the MBA 1590 cm^{-1} peak intensity, (c) 100 × 100 μm^2 SERS map following the spatial distribution of the CuAc 300 cm^{-1} band intensity, and (d) 300 cm^{-1} region where many CuAc bands are present.

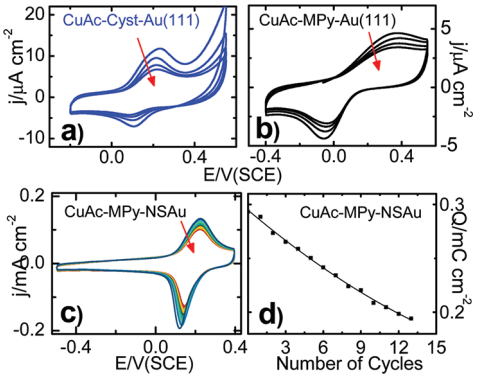

Figure 9. j vs E profiles recorded under repetitive triangular potential scans at $\nu = 0.05$ V s^{-1} for CuAc immobilized on (a) Cyst and (b) MPy SAMs on Au(111). (c) First 13 consecutive potential scans for CuAc immobilized on an MPy SAM on an NSAu substrate. (d) Evolution of the integrated charge in the anodic peak in (c) as a function of the number of cycles. Electrolytic solution: 0.5 M phosphate buffer (pH 7.4).

there are other regions where no peaks used to identify these molecules are observed at all. The most straightforward interpretation of these data is that, first, MBA and HT do not intermix and form SAMs with domains that contain only one kind of molecule and, second, the $-CH_3$ HT terminal group is indeed a nonefficient CuAc trap.

To confirm these conclusions, however, two checks need to be performed. First, it is well-known that NSAu substrates are intrinsically inhomogeneous. Thus, it could also be that the maps in Figure 8 simply express that only regions with high SERS enhancements are detected. To rule out this possibility, we have performed control Raman map experiments with an NSAu substrate modified only with MBA. While, as expected, the SERS intensity was not homogeneous, we have detected the MBA signal throughout the scanned surface, in contrast with the mixed SAM immobilization shown in Figure 8 b,c. This implies that, indeed, the maps in Figure 8 reflect the MBA content at the surface and that red regions can be assigned to MBA and blue regions to HT. The second check to be made is that, in view of the strong dependence of SERS enhancement on the surface—molecule distance, the nonobservation of CuAc in the HT regions might reflect a different location of the CuAc complex with respect to the NSAu substrate for the MBA or HT SAMs. It turns out, however, that both thiol SAMs have very similar thicknesses (MBA, 7.8 Å; HT, 9 Å). Thus, if present, CuAc should be visible when it is immobilized either on MBA or on HT if both thiols are efficient at fixing the complex, something that is not compatible with the green zones in Figure 8d that show the spatial distribution of the CuAc complex in the mixed SAM NSAu substrate. These results thus confirm our conclusions and support the proposal to localize (with micrometer precision) the CuAc complex on patterned surfaces of mixed thiol SAMs with different terminal groups.[81]

3.6. Cu(II)/Cu(I) Electrochemically Induced Delivery. The j vs E profiles recorded under repetitive triangular potential scans for the Cu(II)/Cu(I) redox couple immobilized on Cyst and MPy SAMs on Au(111) exhibit a continuous loss of charge, indicating that Cu(I) species can be slowly delivered from the SAM/electrolyte interface (Figure 9a,b). In contrast, for COOH-terminated SAMs such as MBA and MPA, the charge of the Cu(II)/Cu(I) redox couple remains unchanged during at least 10 potential scans. This means that the N—Cu interaction is weaker than that of O—Cu. Loss of charge in consecutive voltammetric scans of the Cu redox couple has already been shown as an effective method to test the ability to deliver Cu species by photoisomerizable azobenzene ligand in the Au—SAM interface.[82]

On the other hand, the possibility to enhance the capture of CuAc on the SAM-modified NSAu substrates has been shown in the previous section. In Figure 9c we also show that it is possible to electrochemically induce Cu(I) ion delivery from the N donor SAMs on NSAu substrates. As a result, NSAu substrates can act by either trapping and/or delivering from/to the solution significant amounts of Cu(I) species. To show the controlled way in which Cu(I) ions could be delivered from the SAM electrolyte interface, in Figure 9d we present the variation in the integrated charge for the anodic peak of the Cu(II)/Cu(I) redox couple as a function of the number of potential scans for the MPy SAM on the NSAu substrate. For N-terminated thiols a significant (30%) loss of charge is observed after the first 10 repetitive potential scans. Control experiments made by waiting at open circuit potential for time periods comparable to those involved in these potential scans show no changes in the charge involved in the Cu(II)/Cu(I) redox couple. This means that the delivery of Cu ions is electrochemically induced and can be controlled by the applied potential. Note that, under the same experimental conditions, O-terminated thiols do not present significant loss of charge (smaller than 2%). This fact allows performance of a controlled electrochemical delivery of Cu ions from the SAM interface to the solution by tuning the number of electrochemical scans in N-terminated thiol SAMs.

4. CONCLUSIONS AND OUTLOOK

We have immobilized CuAc on different aliphatic and aromatic SAMs of thiols with O and N donors at the end group. Short thiols exhibit high electrochemical activity for the immobilized

Cu ions irrespective of the aliphatic or aromatic character of the molecules because the thinner molecular film allows an easy charge transfer. In the case of long thiols, only a small fraction of the immobilized species are electrochemically active. The efficiency of Cu immobilization on the different SAMs ranges from 26% (for MPy) to 56% (for Cyst) of a complete monolayer of the copper complex. We also show that side products such as free Cu(II) and acetate ions are also incorporated into the SAMs and that they cannot be removed by simple rinsing. This contamination could affect the properties of the SAMs and illustrates the difficulty of controlling the surface chemistry at the nanoscale. This is not a minor issue, with implications on the properties and reproducibility of nanostructured architectures.

We also show that CuAc is spatially oriented on Au(111), suggesting that this simple strategy allows the preparation of complex three-dimensional molecular structures with spatial order. A supramolecular structure, consisting of a second CuAc layer linked by BiPy molecules to the inner first CuAc layer and with the outermost Cu(II) species being able to participate in the charge-transfer process, has also been prepared.

A marked increase in Cu ion capture is observed when nanostructured Au substrates are used where it is also possible to spatially localize, with micrometer precision, Cu ions in domains of mixed thiol SAMs with different terminal groups. In addition, we were able to detect the electroreduction of a fraction of the immobilized Cu(II) species to metallic Cu due to the enhanced stability of the SAMs on this substrate. These results suggest the possibility of controlled electrochemical metallization of SAMs with Cu by improving the SAM−substrate interaction. This strategy could be useful for the formation of the top contacts in molecular electronic devices that use short alkyl or aromatic thiol compounds as the active components. Indeed, it could circumvent the problem of the metallization procedures on SAMs based on evaporation techniques, where penetration of the metal is always found. Controlled release of copper ions to the solution by applying electrical signals is also demonstrated from Au(111) and nanostructured Au substrates.

■ ASSOCIATED CONTENT

Supporting Information. STM image of NSAu and voltammetric curves for CuAc−MUAM SAMs−Au(111), CuAc−MUA SAMs−Au(111), and CuAc−HT SAMs−Au(111). This material is available free of charge via the Internet at http://pubs.acs.org.

■ AUTHOR INFORMATION

Corresponding Author

*E-mail: mevela@inifta.unlp.edu.ar. Phone: +54-221-4257430. Fax: +54-221-4254642.

■ ACKNOWLEDGMENT

We acknowledge financial support from the Agencia Nacional de Promoción Científica y Tecnológica (ANPCyT; Argentina; Grants PICT-2010-2554, PICT-CNPQ 08-019, and PICT06-01061). E.C., N.G.T., A.F., and R.C.S. are also CONICET fellowship and research members. M.E.V. is a research member of the Comisión de Investigaciones Científicas (CIC), Buenos Aires. R.U. is a student of the Sistema de Estudios de Posgrado/Graduate Studies System, Posgrado en Química/Graduate Studies in Chemistry, and Universidad de Costa Rica/University of Costa Rica and a fellow from the Santander Postgraduate Program.

■ REFERENCES

(1) Scodeller, P.; Carballo, R.; Szamocki, R.; Levin, L.; Forchiassin, F.; Calvo, E. J. *J. Am. Chem. Soc.* **2010**, *132*, 11132.
(2) Crumbliss, A. L.; Perine, S. C.; Edwards, A. K.; Rillema, D. P. *J. Phys. Chem.* **1992**, *96*, 1388.
(3) Kind, M.; Wöll, C. *Prog. Surf. Sci.* **2009**, *84*, 230.
(4) Vericat, C.; Vela, M. E.; Benitez, G.; Carro, P.; Salvarezza, R. C. *Chem. Soc. Rev.* **2010**, *39*, 1805.
(5) Love, J. C.; Estroff, L. A.; Kriebel, J. K.; Nuzzo, R. G.; Whitesides, G. M. *Chem. Rev.* **2005**, *105*, 1103.
(6) Bleaney, B.; Bowers, K. D. *Proc. R. Soc. London* **1952**, *214*, 451.
(7) Collman, J. P.; Devaraj, N. K.; Chidsey, C. E. D. *Langmuir* **2004**, *20*, 1051.
(8) Rostovtsev, V. V.; Green, L. G.; Fokin, V. V.; Sharpless, K. B. *Angew. Chem., Int. Ed.* **2002**, *41*, 2596.
(9) Kolb, H. C.; Finn, M. G.; Sharpless, K. B. *Angew. Chem., Int. Ed.* **2001**, *40*, 2004.
(10) Lummerstorfer, T.; Hoffmann, H. *J. Phys. Chem. B* **2004**, *108*, 3963.
(11) Shekhah, O.; Wang, H.; Kowarik, S.; Schreiber, F.; Paulus, M.; Tolan, M.; Sternemann, C.; Evers, F.; Zacher, D.; Fischer, R. A.; Wöll, C. *J. Am. Chem. Soc.* **2007**, *129*, 15118.
(12) Chen, B.; Xiang, S.; Qian, G. *Acc. Chem. Res.* **2010**, *43*, 1115.
(13) Toledo, I.; Arancibia, M.; Andrade, C.; Crivelli, I. *Polyhedron* **1998**, *17*, 173.
(14) Chi, Q.; Zhang, J.; Andersen, J. E. T.; Ulstrup, J. *J. Phys. Chem. B* **2001**, *105*, 4669.
(15) Suzuki, S.; Kataoka, K.; Yamaguchi, K. *Acc. Chem. Res.* **2000**, *33*, 728.
(16) Klis, M.; Maicka, E.; Michota, A.; Bukowska, J.; Sek, S.; Rogalski, J.; Bilewicz, R. *Electrochim. Acta* **2007**, *52*, 5591.
(17) Sunada, K.; Watanabe, T.; Hashimoto, K. *Environ. Sci. Technol.* **2003**, *37*, 4785.
(18) Owens, R. G. *Annu. Rev. Phytopathol.* **1963**, *1*, 77.
(19) Roznyatovskaya, N.; Laurinavichute, V.; Tsirlina, G.; Mirsky, V. *J. Solid State Electrochem.* **2007**, *11*, 981.
(20) Ku, S.-Y.; Wong, K.-T.; Bard, A. J. *J. Am. Chem. Soc.* **2008**, *130*, 2392.
(21) Ivanova, V.; Baunach, T.; Kolb, D. M. *Electrochim. Acta* **2005**, *50*, 4283.
(22) Barth, J. V. *Annu. Rev. Phys. Chem.* **2007**, *58*, 375.
(23) Cortés, E.; Rubert, A. A.; Benitez, G.; Carro, P.; Vela, M. E.; Salvarezza, R. C. *Langmuir* **2009**, *25*, 5661.
(24) Porter, M. D.; Bright, T. B.; Allara, D. L.; Chidsey, C. E. D. *J. Am. Chem. Soc.* **1987**, *109*, 3559.
(25) Ooi, Y.; Hobara, D.; Yamamoto, M.; Kakiuchi, T. *Langmuir* **2005**, *21*, 11185.
(26) Salvarezza, R. C.; Arvia, A. J. A Modern Approach to Surface Roughness Applied to Electrochemical Systems. In *Modern Aspects of Electrochemistry*; White, R. E., Ed.; Plenum Press: New York, 1996; Vol. 28, pp 289−373.
(27) Alonso, C.; Salvarezza, R. C.; Vara, J. M.; Arvia, A. J.; Vazquez, L.; Bartolome, A.; Baro, A. M. *J. Electrochem. Soc.* **1990**, *137*, 2161.
(28) Vazquez, L.; Bartolome, A.; Baro, A. M.; Alonso, C.; Salvarezza, R. C.; Arvia, A. J. *Surf. Sci.* **1989**, *215*, 171.
(29) Vela, M. E.; Zerbino, J. O.; Arvia, A. J. *Thin Solid Films* **1993**, *233*, 82.
(30) Macchi, C.; Somoza, A.; Mariazzi, S.; Brusa, R. S.; Vericat, C.; Vela, M. E.; Salvarezza, R. C. *Phys. Status Solidi C* **2009**, *6*, 2585.
(31) Vericat, C.; Benitez, G. A.; Vela, M. E.; Salvarezza, R. C.; Tognalli, N. G.; Fainstein, A. *Langmuir* **2006**, *23*, 1152.
(32) Vela, M. E.; Martin, H.; Vericat, C.; Andreasen, G.; Hernandez Creus, A.; Salvarezza, R. C. *J. Phys. Chem. B* **2000**, *104*, 11878.

(33) Saavedra, H. c. M.; Thompson, C. M.; Hohman, J. N.; Crespi, V. H.; Weiss, P. S. *J. Am. Chem. Soc.* **2009**, *131*, 2252.
(34) Laibinis, P. E.; Bain, C. D.; Whitesides, G. M. *J. Phys. Chem.* **1991**, *95*, 7017.
(35) Upadhyay, D. N.; Yegnaraman, V.; Rao, G. P. *Langmuir* **1996**, *12*, 4249.
(36) Yang, W.; Justin Gooding, J.; Brynn Hibbert, D. *J. Electroanal. Chem.* **2001**, *516*, 10.
(37) Finklea, H. Electrochemistry of Organized Monolayers of Thiols and Related Molecules on Electrodes. In *Electroanalytical Chemistry*; Bard, A. J., Rubinstein, I., Eds.; Marcel Dekker: New York, 1996; Vol. 19, pp 110−318.
(38) *Electrochemical Methods: Fundamentals and Applications*; Bard, A. J., Faulkner, L. R., Eds.; Wiley & Sons: New York, 2001; pp 590−595.
(39) Laviron, E. *J. Electroanal. Chem.* **1979**, *100*, 263.
(40) Eckermann, A. L.; Feld, D. J.; Shaw, J. A.; Meade, T. J. *Coord. Chem. Rev.* **2010**, *254*, 1769.
(41) Repo, E.; Ahlberg, E.; Murtomäki, L.; Kontturi, K.; Schiffrin, D. J. *Electrochim. Acta* **2009**, *54*, 6584.
(42) Petri, M.; Kolb, D. M.; Memmert, U.; Meyer, H. *Electrochim. Acta* **2003**, *49*, 175.
(43) Cui, Y.; Yang, C.; Zeng, W.; Oyama, M.; Pu, W.; Zheng, Y.; Zhang, J. *Anal. Lett.* **2007**, *40*, 2151.
(44) Zangmeister, C. D.; Bertocci, U.; Beauchamp, C. R.; Stafford, G. R. *Electrochim. Acta* **2008**, *53*, 6778.
(45) Zhang, J.; Bilic, A.; Reimers, J. R.; Hush, N. S.; Ulstrup, J. *J. Phys. Chem. B* **2005**, *109*, 15355.
(46) Wirde, M.; Gelius, U.; Nyholm, L. *Langmuir* **1999**, *15*, 6370.
(47) Sawaguchi, T.; Mizutani, F.; Yoshimoto, S.; Taniguchi, I. *Electrochim. Acta* **2000**, *45*, 2861.
(48) Zhou, W.; Baunach, T.; Ivanova, V.; Kolb, D. M. *Langmuir* **2004**, *20*, 4590.
(49) Kakiuchi, T.; Usui, H.; Hobara, D.; Yamamoto, M. *Langmuir* **2002**, *18*, 5231.
(50) Iwami, Y.; Hobara, D.; Yamamoto, M.; Kakiuchi, T. *J. Electroanal. Chem.* **2004**, *564*, 77.
(51) Aguilar-Sanchez, R.; Su, G. J.; Homberger, M.; Simon, U.; Wandlowski, T. *J. Phys. Chem. C* **2007**, *111*, 17409.
(52) Kunze, J.; Leitch, J.; Schwan, A. L.; Faragher, R. J.; Naumann, R.; Schiller, S.; Knoll, W.; Dutcher, J. R.; Lipkowski, J. *Langmuir* **2006**, *22*, 5509.
(53) Wühn, M.; Weckesser, J.; Woll, C. *Langmuir* **2001**, *17*, 7605.
(54) Chusuei, C. C.; Brookshier, M. A.; Goodman, D. W. *Langmuir* **1999**, *15*, 2806.
(55) Baio, J. E.; Weidner, T.; Brison, J.; Graham, D. J.; Gamble, L. J.; Castner, D. G. *J. Electron Spectrosc. Relat. Phenom.* **2009**, *172*, 2.
(56) Stettner, J.; Winkler, A. *Langmuir* **2010**, *26*, 9659.
(57) Calvo, E. J.; Rothacher, M. S.; Bonazzola, C.; Wheeldon, I. R.; Salvarezza, R. C.; Vela, M. E.; Benitez, G. *Langmuir* **2005**, *21*, 7907.
(58) de Meester, P.; Fletcher, S. R.; Skapski, A. C. *J. Chem. Soc., Dalton Trans.* **1973**, 2575.
(59) Takagi, H.; Mikata, Y.; Ichimura, A.; Yano, T.; Kinoshita, I.; Hori, M.; Collins, T. J.; Gottschaldt, M.; Yano, S. *Electrochim. Acta* **2009**, *54*, 1286.
(60) Kolat, R. S.; Powell, J. E. *Inorg. Chem.* **1962**, *1*, 293.
(61) Freire, R. S.; Kubota, L. T. *Electrochim. Acta* **2004**, *49*, 3795.
(62) Vishweshwar, P.; Nangia, A.; Lynch, V. M. *J. Org. Chem.* **2001**, *67*, 556.
(63) Cecchet, F.; Fioravanti, G.; Marcaccio, M.; Margotti, M.; Mattiello, L.; Paolucci, F.; Rapino, S.; Rudolf, P. *J. Phys. Chem. B* **2005**, *109*, 18427.
(64) Chah, S.; Yi, J.; Pettit, C. M.; Roy, D.; Fendler, J. H. *Langmuir* **2001**, *18*, 314.
(65) Schäfer, A. H.; Seidel, C.; Chi, L.; Fuchs, H. *Adv. Mater.* **1998**, *10*, 839.
(66) Neuert, G.; Kufer, S.; Benoit, M.; Gaub, H. E. *Rev. Sci. Instrum.* **2005**, *76*, 054303.
(67) Brockman, J. M.; Frutos, A. G.; Corn, R. M. *J. Am. Chem. Soc.* **1999**, *121*, 8044.
(68) Kučera, J.; Gross, A. *Langmuir* **2008**, *24*, 13985.
(69) Wagner, P.; Hegner, M.; Güntherodt, H. J.; Semenza, G. *Langmuir* **1995**, *11*, 3867.
(70) Lee, J. R. I.; Willey, T. M.; Nilsson, J.; Terminello, L. J.; De Yoreo, J. J.; van Buuren, T. *Langmuir* **2006**, *22*, 11134.
(71) Dubois, C.; Stellacci, F. *J. Phys. Chem. C* **2008**, *112*, 7431.
(72) Zhang, J.; Kuznetsov, A. M.; Medvedev, I. G.; Chi, Q.; Albrecht, T.; Jensen, P. S.; Ulstrup, J. *Chem. Rev.* **2008**, *108*, 2737.
(73) Fujita, K.; Nakamura, N.; Ohno, H.; Leigh, B. S.; Niki, K.; Gray, H. B.; Richards, J. H. *J. Am. Chem. Soc.* **2004**, *126*, 13954.
(74) Mendes, R. K.; Freire, R. S.; Fonseca, C. P.; Neves, S.; Kubota, L. T. *J. Braz. Chem. Soc.* **2004**, *15*, 849.
(75) Xu, B.; Tao, N. J. *Science* **2003**, *301*, 1221.
(76) Pérez-Jiménez, Á. J. *J. Phys. Chem. B* **2005**, *109*, 10052.
(77) Yang, Z.; Engquist, I.; Liedberg, B.; Kauffmann, J.-M. *J. Electroanal. Chem.* **1997**, *430*, 189.
(78) Silien, C.; Buck, M. *J. Phys. Chem. C* **2008**, *112*, 3881.
(79) Michota, A.; Bukowska, J. *J. Raman Spectrosc.* **2003**, *34*, 21.
(80) Mathey, Y.; Greig, D. R.; Shriver, D. F. *Inorg. Chem.* **1982**, *21*, 3409.
(81) Garno, J. C.; Zangmeister, C. D.; Batteas, J. D. *Langmuir* **2007**, *23*, 7874.
(82) Takahashi, I.; Honda, Y.; Hirota, S. *Angew. Chem., Int. Ed.* **2009**, *48*, 6065.